nature portfolio

https://doi.org/10.1038/s41586-023-06596-2

Supplementary information

Cavity-mediated thermal control of metal-to-insulator transition in 1T-TaS_2

In the format provided by the authors and unedited

SUPPLEMENTARY MATERIAL

1. **Addressing specific questions arising**
   "Is the observed effect related to incoherent radiation heating or can be associated to the cavity electrodynamics?"

   a. Does the presence of the sample affect the difference between the temperature of the cold finger and the temperature in the middle of the cavity?
   b. Does the temperature of the cavity mirrors affect the sample temperature?
   c. Does the alignment of the cavity modify the sample temperature?
   d. Does the external radiation influence the sample temperature?
   e. Does the thermal load of the THz radiation affect the observed transition temperature?

2. **Additional datasets**

1. ADDRESSING SPECIFIC QUESTIONS ARISING

The main experimental evidence reported in the manuscript is that the effective critical temperature of the metal-to-insulator transition in 1T-TaS_2 can be modified by tens of kelvin by placing the sample within a THz cavity. This is linked to a cavity control of the sample temperature, as demonstrated in the main manuscript. We have proved that the observed temperature renormalization depends both on the cavity length and the cavity alignment.

The novelty of the experiment, which represents one of the few attempts in the literature to study how the properties of solid-state complex systems can be modified through the cavity confinement, calls for a thorough characterization of the effect with the aim of ruling out possible experimental artifacts and trivial scenarios. In particular, the most straightforward explanation could be that the huge shift of the effective critical temperature is due to an incoherent radiation heating of the sample, placed within the cavity and therefore in scarce thermal contact with the cold finger.

In the following, we will detail that this is not the case. By jointly discussing results of the finite elements simulations and the temperature measurements, we will give proves pointing towards cavity electrodynamics as the dominant effect explain our experimental observations.

To facilitate the discussion, we will address specific questions that may arise and argue how the complementary tests that we carried out hint towards a cavity-mediated scenario.

a. Does the presence of the sample affect the difference between the temperature of the cold finger and the temperature in the middle of the cavity?

In a trivial scenario in which the sample experiences an incoherent radiation heating, also the membranes are expected to behave similarly in response to the modification of the cavity geometry. In order to rule out this possibility, we measured the temperature of the sample and the temperature of just the membranes (i.e., without placing the sample between them) by means of the micrometric thermocouple for different cavity fundamental modes.

Fig. S1 presents the results of the temperature measurements performed within the cavity when the thermocouple is sealed on the sample (Fig. S1(A)) and when it is held just between the two membranes (Fig. S1(B)). The temperature measurements, for each cavity setting, are plotted as the difference between the temperature measured on the sample/membrane ($T_{int}/T_{membrane}$) and the one recorded on the cold finger (T_{ext}) as function of T_{int} or $T_{membrane}$.

We highlight two distinctive trends, characteristic of the presence of the sample:

- The absolute temperature renormalization passing from the lower to higher cavity frequency is significantly higher on the sample with respect to the membrane. For the lowest cold finger temperature (T_{ext} = 80 K) we indeed measured a renormalization of the sample's temperature of ~ 27 K moving the cavity fundamental mode from 11.5 GHz to 42.8 GHz. Conversely, between the two cavity configurations we measured only a ~ 9 K renormalization of the membrane's temperature.

- The temperature renormalization induced by the cavity in the sample is non-monotonic with respect to the free-space case. Indeed, for high frequency cavities the sample's temperature within the cavity is lower with respect to the sample's temperature measured in free space. This is qualitatively consistent with the trend of the effective critical temperature as function of the cavity fundamental mode revealed by THz spectroscopy (Fig. 4A). Conversely, this anomalous non-monotonic behaviour is not observed on the membranes, where the membrane's temperature measured within the cavity is lower than the free space case for all the cavity frequencies studies. In particular, we observe that the

membrane's temperature measured for the larger cavity length (11.5 GHz) approaches the trend measured in free space.

In Fig. S1(C) we present the differential temperature $T_{int} - T_{ext}$ for a fixed cold finger temperature (T_{ext} = 150 K) as a function of the cavity fundamental frequency. As expected from full temperature scans presented in Fig. S1(A, B) we revealed a renormalization of the sample's effective temperature of ~18 K by sweeping the cavity mode from 11.5 GHz to 42.8 GHz. On the other hand, for the same frequency range, we detected a significantly smaller change in the membrane temperature (~ 5 K).

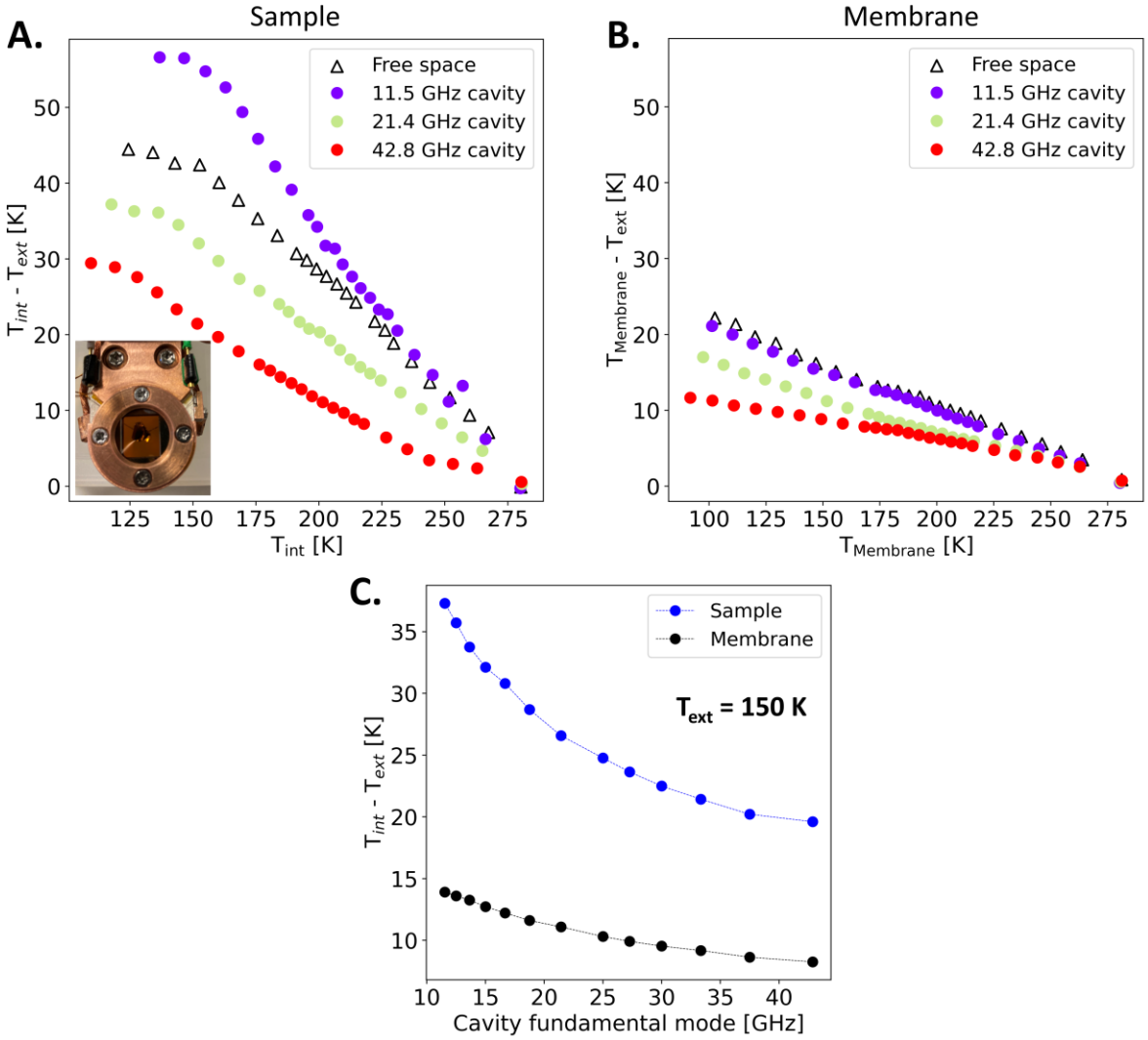

Fig S1: Temperature measurements within the cavity. **A.** Difference between the temperature measured on the sample (T_{int}) and on the cold finger (T_{ext}) as a function of the sample temperature. Temperatures have been measured upon heating the sample from the C-CDW phase. **B.** Difference between the membrane's temperature and the cold finger temperature when the thermocouple is held just between the two membranes. **C.** Difference between the temperature measured on the thermocouple and on the cold finger as a function of the cavity frequency for a fixed cold finger temperature (T_{ext} = 150 K). In blue the measurements performed with the thermocouple put on the sample, while in black with the thermocouple held between the membranes.

A further confirmation that the reported effect hints towards a cavity-mediated scenario comes from the direct measurement of the sample's temperature both in heating and cooling conditions. Should the temperature renormalization depend on an incoherent heating, no differences would be expected in the two scanning

conditions. This is in fact what we observed on the membranes (Fig. S2(A)), where the difference between $T_{membrane}$ and T_{ext} is identical when heating up or cooling down within the cavity. However, the sample's temperature shows a different trend for the heating/cooling directions (Fig. S2(B)). In particular, while we do not observe any systematic discontinuity when heating up the sample, a kink at the nominal critical temperature ~ 215 K is always present when cooling down the sample at different cavity lengths. In the temperature range ~ 160-215 K we also observe a constant temperature difference between the sample and the cold finger. The thermodynamical meaning of this effect is not clear, but the observation of this hysteretic behaviour, which is not present on the bare membranes, proves that all the effects discussed are peculiar of the sample.

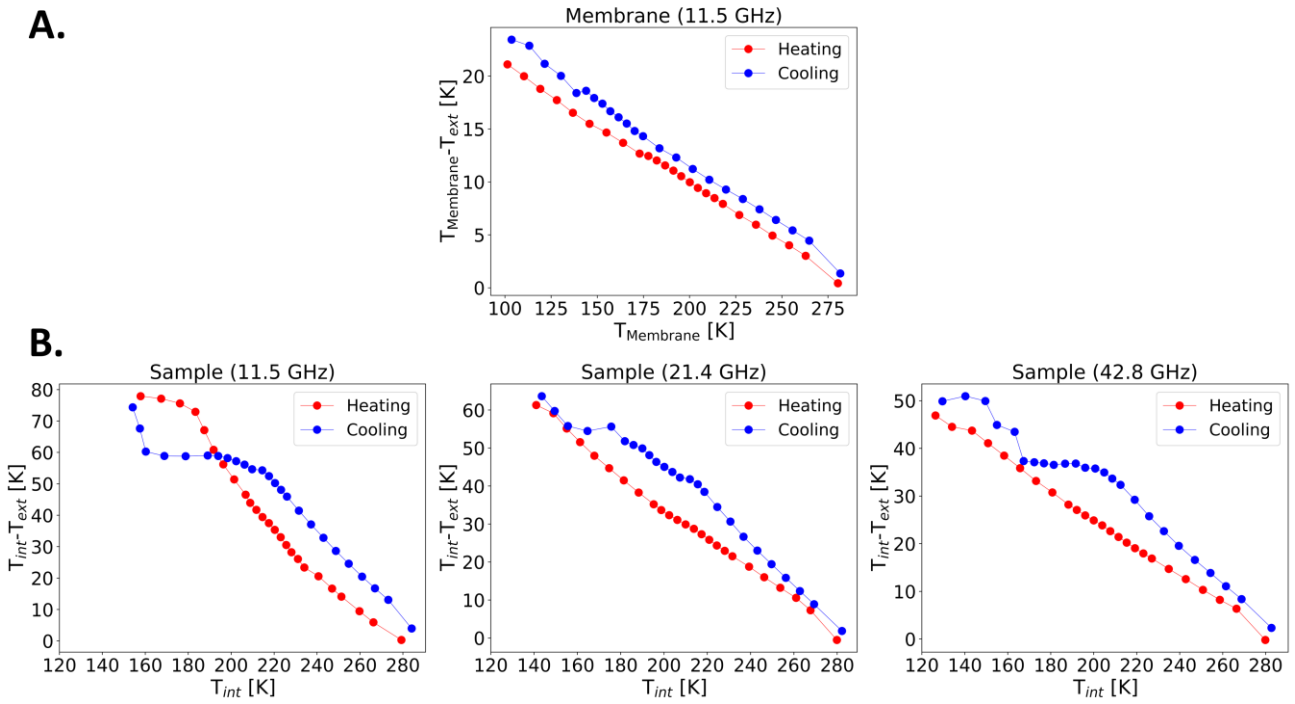

Fig S2: Temperature measurements upon heating and cooling. A. Difference between the membrane and the cold finger temperature within a 11.5 GHz cavity upon heating (red curve) and cooling (blue curve). **B.** Same as (A) but for the sample's temperature in three different cavity configurations.

b. Does the temperature of the cavity mirrors affect the sample temperature?

A possible source of incoherent thermal load are the cavity mirrors, whose presence might affect the temperature of the sample. In order to exclude this incoherent heating scenario, we carried out a characterization of the phase transition shift with cavity frequency as a function of the mirrors temperature. We made this test by comparing the cryo-cooled (T = 95 K[1]) mirrors configuration with the 290 K mirrors one. The relation between the mirrors and the sample's temperature in the two cases is presented in Fig. S3.

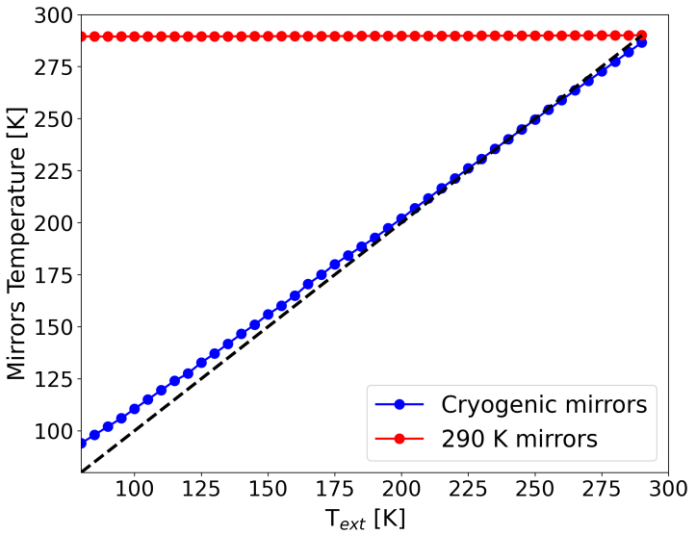

Fig S3: Relation between the sample temperature and the mirrors temperature in the cryo-cooled mirrors configuration and in the 290 K mirrors configuration. The black dashed line marks the diagonal.

Fig. S4 shows the temperature dependent THz transmission upon heating 1T-TaS_2 embedded in the middle of cavities with three different frequencies (ω_c = 11.5, 21.2, 48.8 GHz). In Fig. S4(A) the temperature scans were performed with the cavity mirrors at 290 K, while in Fig. S4(B) they were performed in the configuration with cryo-cooled mirrors. The dependence of the effective critical temperature (T_c^{eff}) on the cavity frequency is presented in Fig S5 for the two configurations.

It is evident that, despite a rigid temperature shift independent on the cavity frequency (~ 35 K), the effective critical temperature of the phase transition is pushed up with the 290 K mirrors upon increasing the cavity frequency, displaying a trend which is analogous to the one measured with the cryo-cooled mirrors. Crucially, this evidence further hints that the observed shift of T_c^{eff} is an effect due to the cavity confinement. In a trivial incoherent heating scenario, in the 290 K mirrors configuration we would have expected to increase the incoherent thermal load on the sample upon closing the cavity and hence push down the apparent critical temperature of the phase transition.

[1] This is the lowest reachable temperature of the mirrors for the present experiment, measured when the cold finger is at T_{ext} = 80 K.

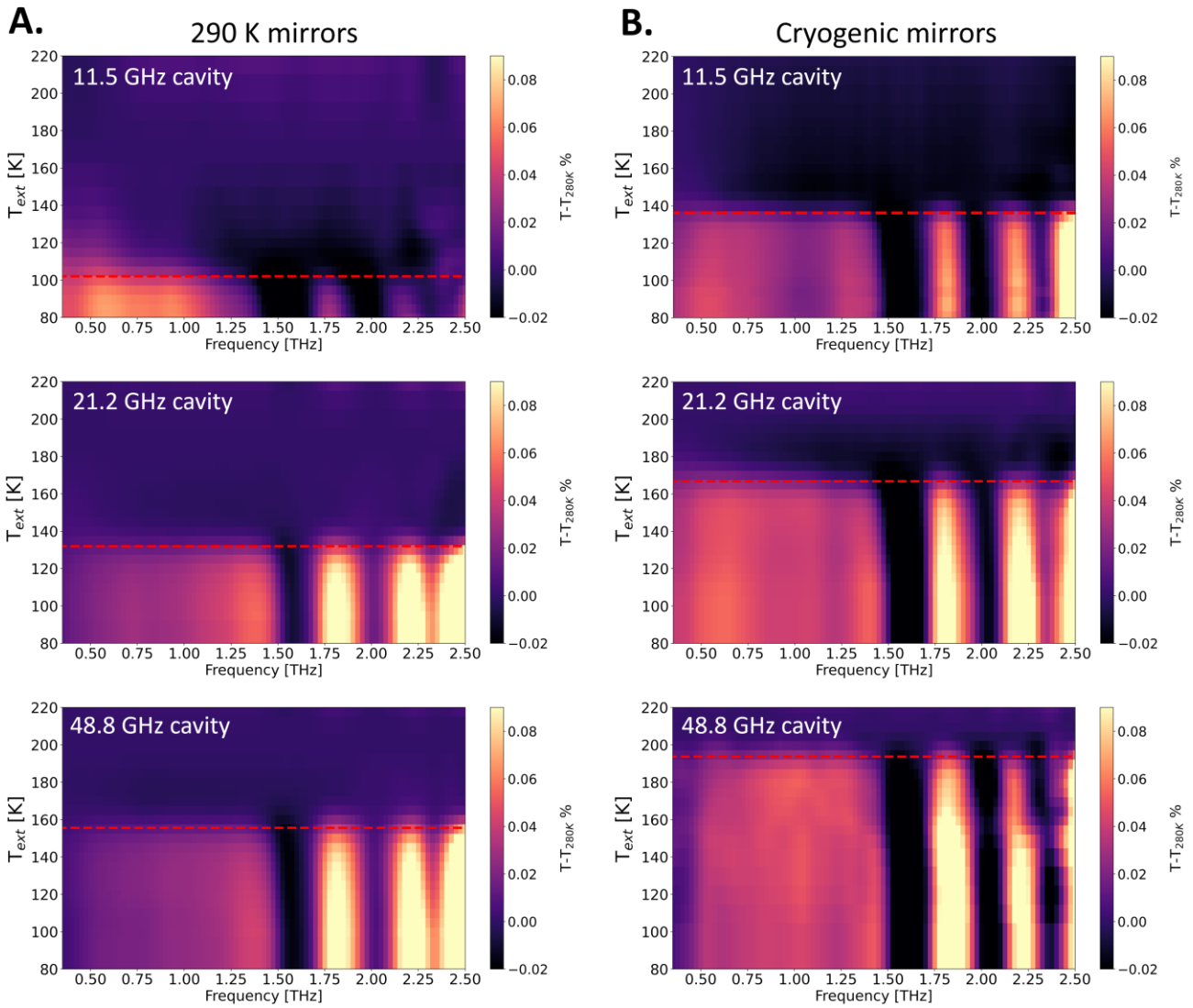

Fig S4: Dependence of the effective phase transition temperature on the temperature of the cavity mirrors revealed by THz spectroscopy. **A.** Heating temperature scans for three representative cavity frequencies (ω_c = 11.5, 21.2, 48.8 GHz) in the 290 K mirrors configuration. **B.** Corresponding heating temperature scans for the cryogenic mirrors configuration.

In order to clarify this point, we simulated with COMSOL the membrane's thermal profile embedded in three cavities having different lengths. The employed 3D geometry can be found in Fig. S6(A) and Fig. S7(A) for cryogenic and ambient temperature mirrors, respectively.
The radial profiles plotted in Fig. S6(C) and Fig. S7(C) show that, upon closing the cavity and thus increasing the cavity frequency, the shielding of ambient radiation is efficient only with the cryogenic mirrors, whereas in the 300 K mirror case the incoherent radiation from the mirrors surfaces dominates the thermal load on the membrane. We stress that this trend is opposite to the one measured by THz spectroscopy (Fig. S4, S5).

Together with THz transmission, we characterized the effect of the mirrors temperature on the phase transition by tracking the sample's temperature as a function of the cavity length and of the cavity alignment. Fig. S8 shows a comparison of the differential temperature between the cold finger and the sample when the latter is held between the cryogenic cavity (Fig. S8(A)) and between the cavity with 290 K mirrors (Fig. S8(B)). The measured trend is qualitatively consistent with the effective critical temperature trend measured by THz spectroscopy (Fig. S5). Indeed, despite a cavity-independent shift of the sample's temperature due to the

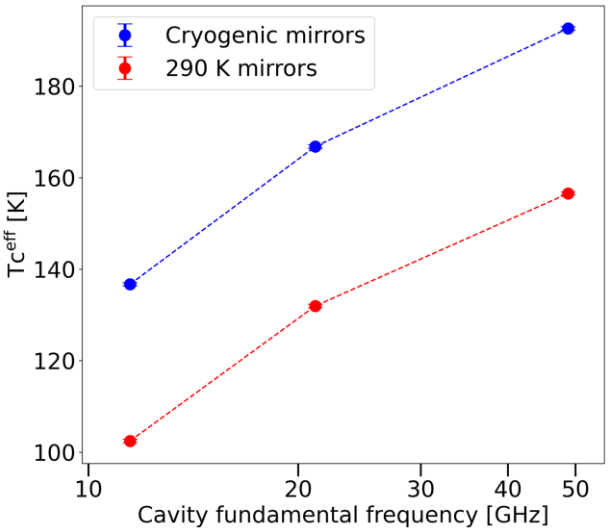

Fig S5: Dependence of the heating critical temperature on the cavity fundamental frequency for the 290 K and cryogenic mirrors configurations. In blue (red) the effective critical temperature measured upon heating the sample from the dielectric phase for the cryogenic mirrors (290 K mirrors) configuration.

incoherent thermal load, in the 290 K mirrors case the sample's temperature is pushed down with a similar trend of the cryogenic mirrors case upon increasing the cavity frequency.

For the lowest cold finger temperature (T_{ext} = 80 K) and in the 290 K mirrors case we measured a renormalization of the sample's temperature of ~ 31 K by sweeping the cavity mode from 11.5 GHz to 42.8 GHz, which is similar to the ~ 27 K measured within the cryogenic cavity. A similar trend between the 290 K and cryo-cooled cases is measured by fixing the cold finger at 150 K and tracking the differential temperature $T_{int} - T_{ext}$ as a function of the cavity fundamental mode (Fig. S8(C)). As highlighted in the comparative plots of Fig. S8(C), the renormalization of the sample's temperature measured either within the cryogenic cavity and with the 290 K mirrors is not consistent with the trend measured on the bare membranes, where a ~ 3 times smaller renormalization is observed moving the cavity mode at 150 K from 11.5 GHz to 42.8 GHz (black points of Fig. S8(C)).

Crucially, we further proved that the cavity-mediated change of sample's temperature is independent on the mirrors temperature by repeating the misalignment test with the 290 K mirrors. In Fig. S9 we present the comparison of the differential temperature $T_{int} - T_{ext}$ as function of the cavity alignment in the cryo-cooled and in the 290 K mirrors case. We show that, despite a rigid shift due to the incoherent thermal load introduced by the 290 K mirrors, the renormalization of the sample's temperature due to the cavity alignment is ~ 3.5 times larger than the one measured on the bare membranes for both the mirrors temperature configurations. This evidence further excludes that the observed effect is related to the mirror's incoherent heating and hints to a selective effect of the cavity electrodynamics on the sample's temperature.

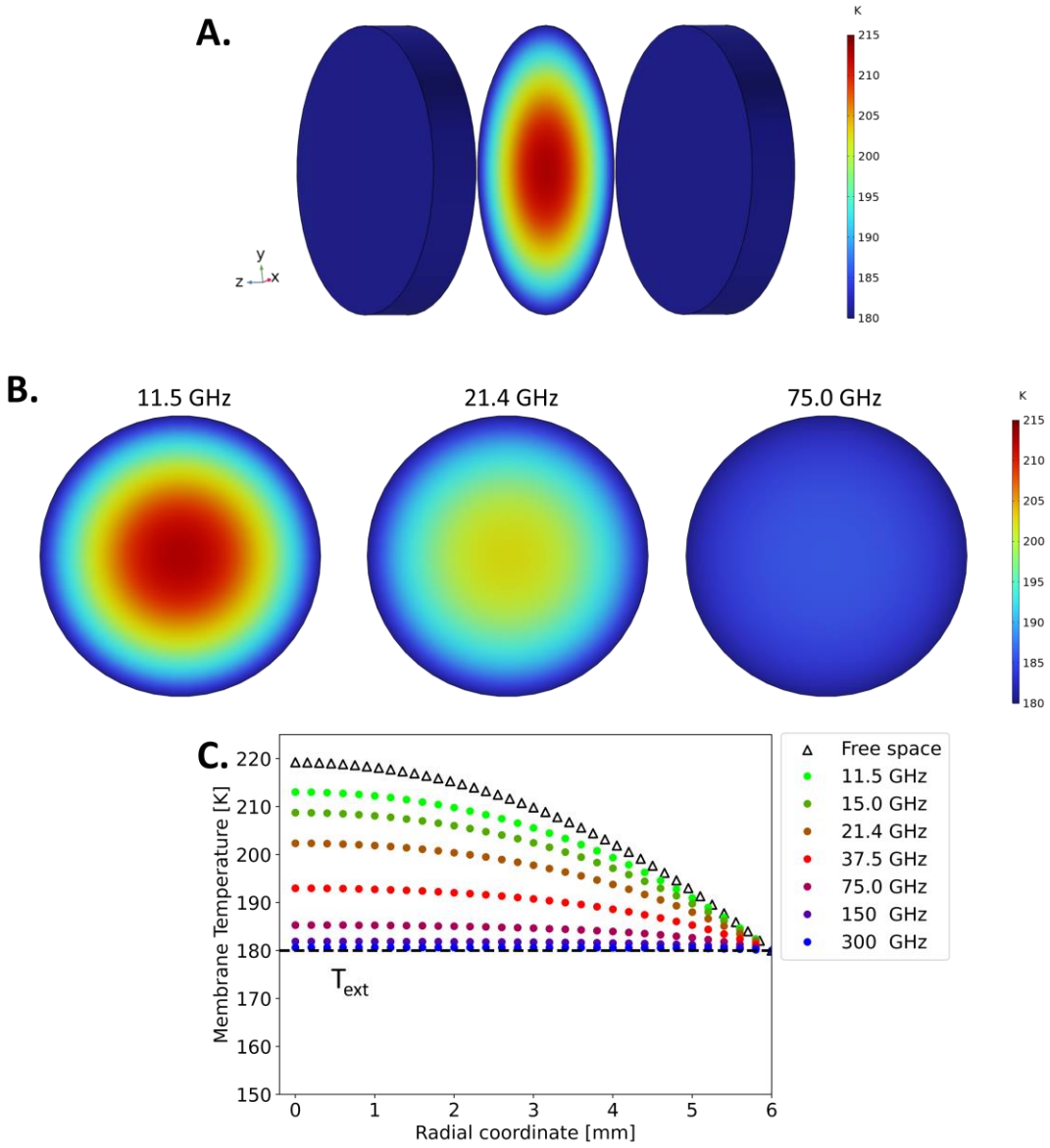

Fig S6: Finite elements simulation of membrane's temperature as a function of the cavity fundamental frequency in the cryogenic mirrors configuration. A. 3D thermal view of the cryogenic cavity employed for the simulations. **B.** 2D thermal profile of the membrane within the cryogenic cavity for three representative cavity frequencies (11.5, 21.4, 75.0 GHz) employed in the experiment. **C.** Radial profile of the membranes held within the cryogenic cavity for different values of the cavity fundamental mode (indicated in legend). The cold finger temperature (T_{ext}) and the mirrors temperature have been set at 180 K.

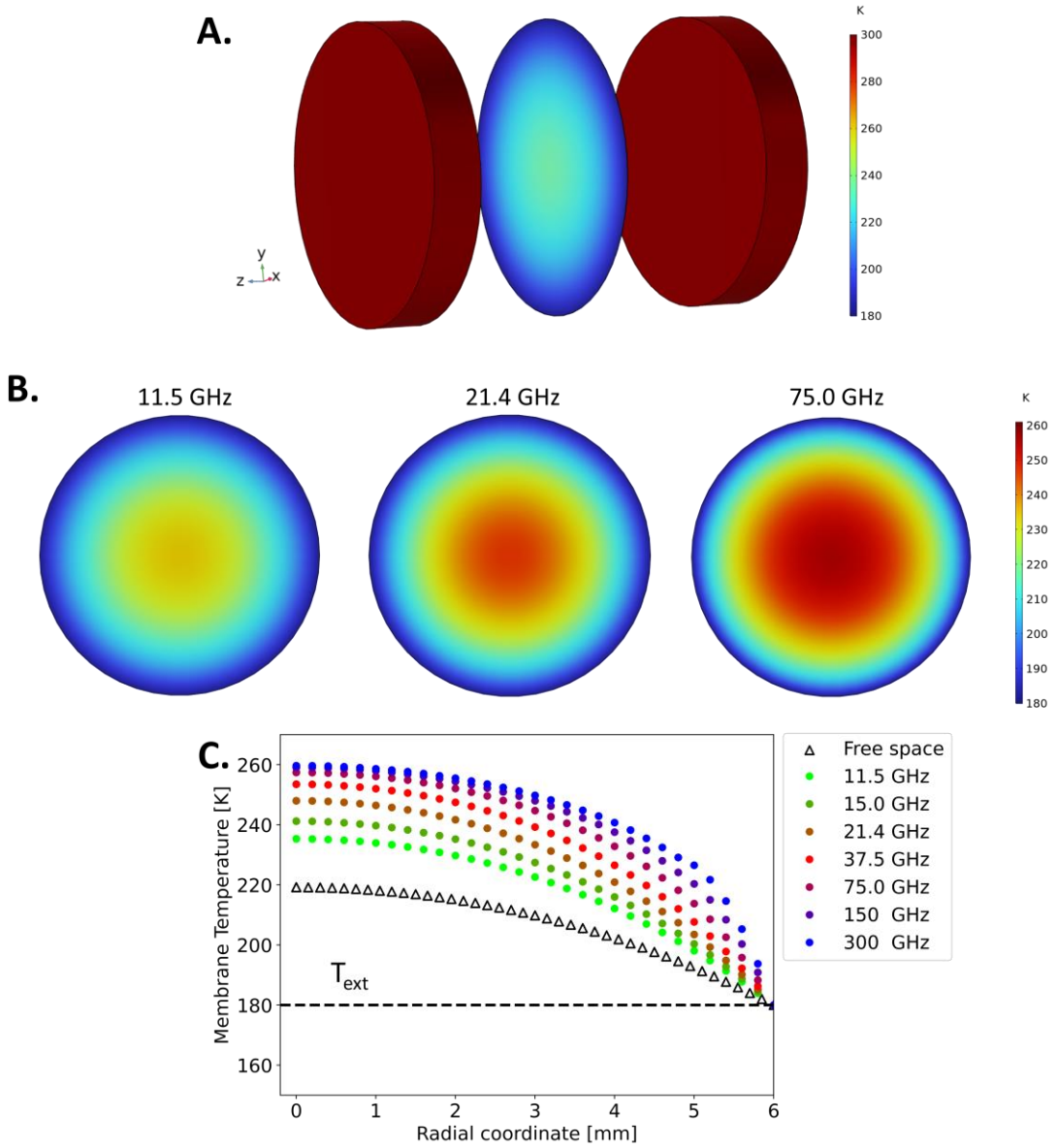

Fig S7: Finite elements simulation of membrane's temperature as a function of the cavity fundamental frequency in the 300 K mirrors configuration. A. 3D thermal view of the membrane held between the 300 K mirrors. **B.** 2D thermal profile of the membrane within the 300 K mirrors for three representative cavity frequencies (11.5, 21.4, 75.0 GHz) employed in the experiment. **C.** Radial profile of the membranes in the 300 K mirrors configuration for different values of the cavity fundamental mode (indicated in legend). The cold finger temperature (T_{ext}) has been set to 180 K.

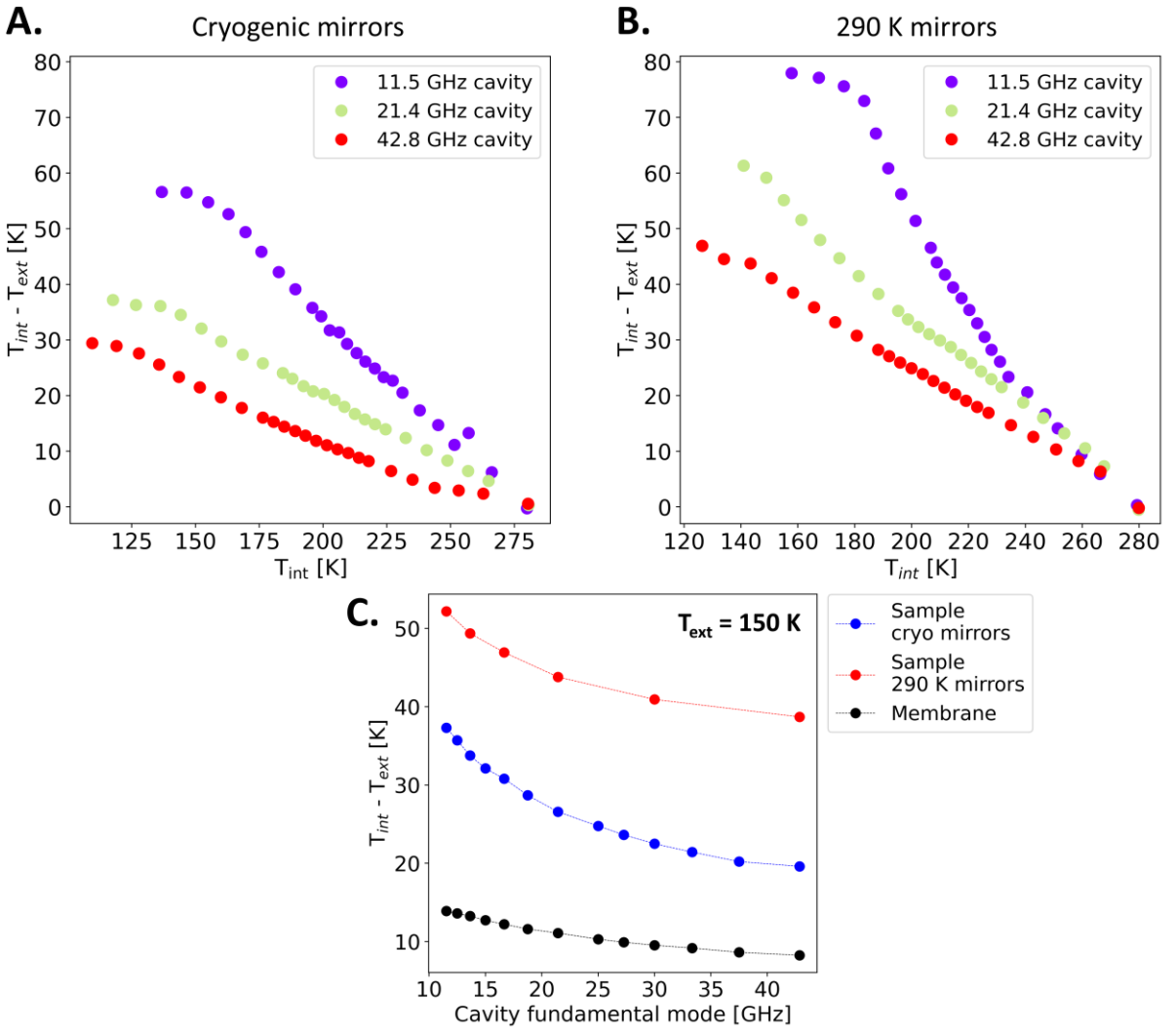

Fig S8: Temperature measurement within the cavity as a function of the mirrors temperature. A. Evolution of the difference between the temperature measured on the sample (T_{int}) and on the cold finger (T_{ext}) as a function of the sample temperature in the cryo-cooled mirrors configuration. **B.** Differential temperature $T_{int} - T_{ext}$ as a function of the sample's temperature measured in the 290 K mirrors configuration. In both cases the temperatures have been measured upon heating the sample from the C-CDW phase. **C.** Differential temperature $T_{int} - T_{ext}$ for a fixed cold finger temperature (T_{ext} = 150 K) as a function of the cavity fundamental frequency. In blue the measurements performed within the cavity with cryogenic mirrors, while in red with 290 K mirrors. In black, for reference, the differential temperature measured within the membranes in the cryogenic mirrors configuration.

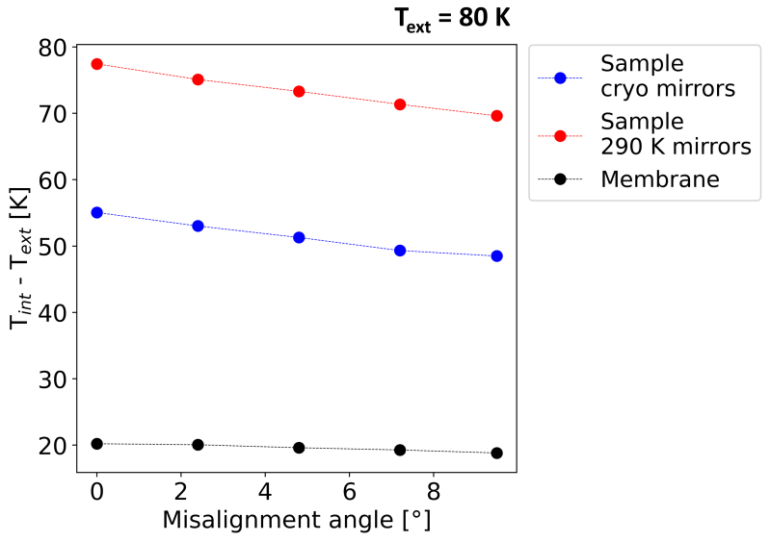

Fig S9: Temperature measurements within the cavity as a function of the cavity alignment for different mirror temperatures. Differential temperature $T_{int} - T_{ext}$ as a function of the alignment measured for the sample held within cryogenic mirrors (blue) and 290 K mirrors (red). In black, for comparison, the differential temperature measured on the membranes. For the present measurements the cold finger has been set at T_{ext} = 80 K.

c. Does the alignment of the cavity modify the sample temperature?

A further parameter which was shown to affect the effective critical temperature of the metal-to-insulator transition is the alignment of the cavity, which ultimately sets its quality factor (Fig. 3B of the main manuscript). In order to demonstrate that this is not just a pure geometrical effect, we characterize in the following the response of the sample to the cavity misalignment.

First of all, we proved that the effective change of the phase transition temperature due to the cavity alignment cannot be ascribed to a change of the cavity length. In order to do so, we estimated the change of the cavity frequency at the sample position as a function of the misalignment angle of the mirrors. Fig. S10(A) illustrates the THz time-domain traces in the C-CDW phase for different misalignment angles Θ. In the dashed box we highlight the THz reflection associated to the cavity round trip whose temporal distance from the main transmitted peak sets the cavity length. We note that upon misalignment the peak associated to the cavity round trip reduces its intensity. This is consistent with the decrease of the photon lifetime within the cavity and hence with the reduction of the quality factor of the bare cavity, which has been estimated in Fig. S10(B) as a function of the misalignment angle by approximating the exponential decay with a linear fit.

The dependence of the cavity frequency shift on Θ and the corresponding linear fit are shown in Fig. S10(C). We estimated the change of the fundamental frequency upon misalignment to be $\Delta\omega_c$ = 0.14 GHz/deg for the 11.5 GHz cavity. This implies that the 11.5 GHz cavity misaligned at the maximum angle (Θ = 9.5°) has an equivalent fundamental frequency of 12.8 GHz. We therefore set the cavity frequency at 12.8 GHz and compare the effective critical temperature obtained in this configuration with the one of the sample embedded within the 11.5 GHz cavity misaligned at Θ = 9.5°. We measured the shift of the effective critical temperature between the two cavity configurations to be Δ_{MIS} = 21 K. The apparent shift of the phase transition can be hence attributed to the cavity misalignment (Fig. S10(D)), as it cannot be justified just in terms of a change in the cavity length.

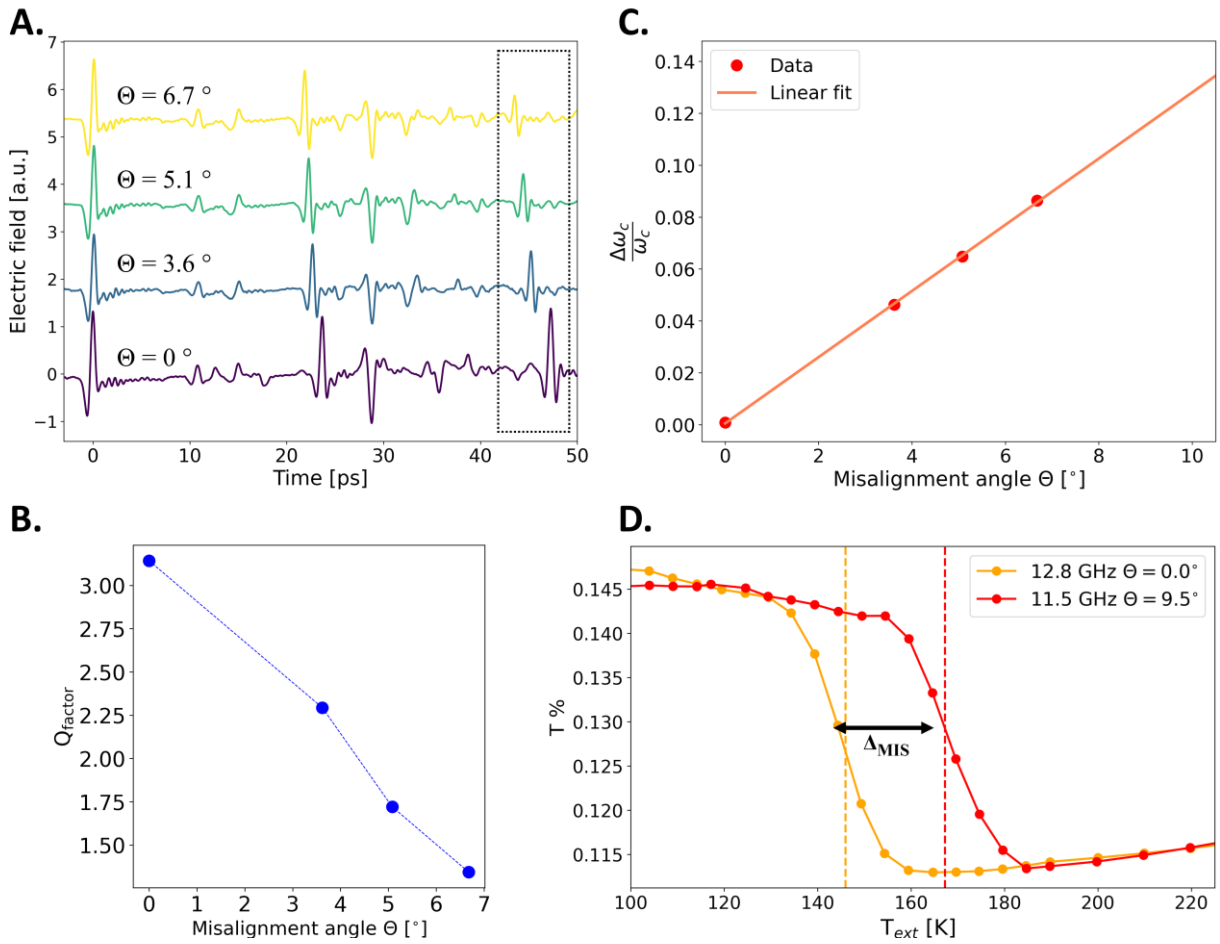

Fig S10: Variation of the cavity fundamental frequency as a function of the total misalignment angle of the cavity. **A.** THz time domain fields passing through the sample within the cavity for different misalignment angles Θ. In the dashed box we highlight the THz reflection associated to the cavity round trip. **B.** Estimated cavity quality factor as a function of the misalignment angle. **C.** Relative shift of the cavity frequency as a function of the misalignment angle obtained from the THz fields shown in A and corresponding linear fit. **D.** Comparison between the temperature dependent low frequency transmission (0.2 THz < ω < 1.5 THz) in the 11.5 GHz misaligned cavity (Θ = 9.5°) and in the 12.8 GHz aligned one. The measured temperature shift Δ_{MIS} = 21 K quantifies the shift of the effective critical temperature T_c^{eff} due to cavity misalignment.

Furthermore, by means of the finite elements simulations, we proved that the renormalization of the effective critical temperature cannot be explained by simply assuming an incoherent thermal heating. In fact, as shown in Fig. S11, no temperature shift in the membrane is expected when the cavity mirrors are in the maximum misaligned configuration considered in the experiment (θ = 9.5°).

Finally, in order to verify how the sample's temperature is affected by the cavity environment, we measured T_{int} as a function of the cavity alignment for a cavity fundamental mode of 11.5 GHz (Fig. S12). By setting the cold finger temperature to 80 K, we detected a renormalization of 6.5 K in the sample's temperature by switching from the aligned to the maximum misaligned condition. Conversely, we measured only a 1.6 K temperature variation when the thermocouple is held only between the two membranes. We note that the measured renormalization of the sample's temperature is much smaller than the shift of the effective transition temperature measured by THz spectroscopy (Fig. 3 in the main).

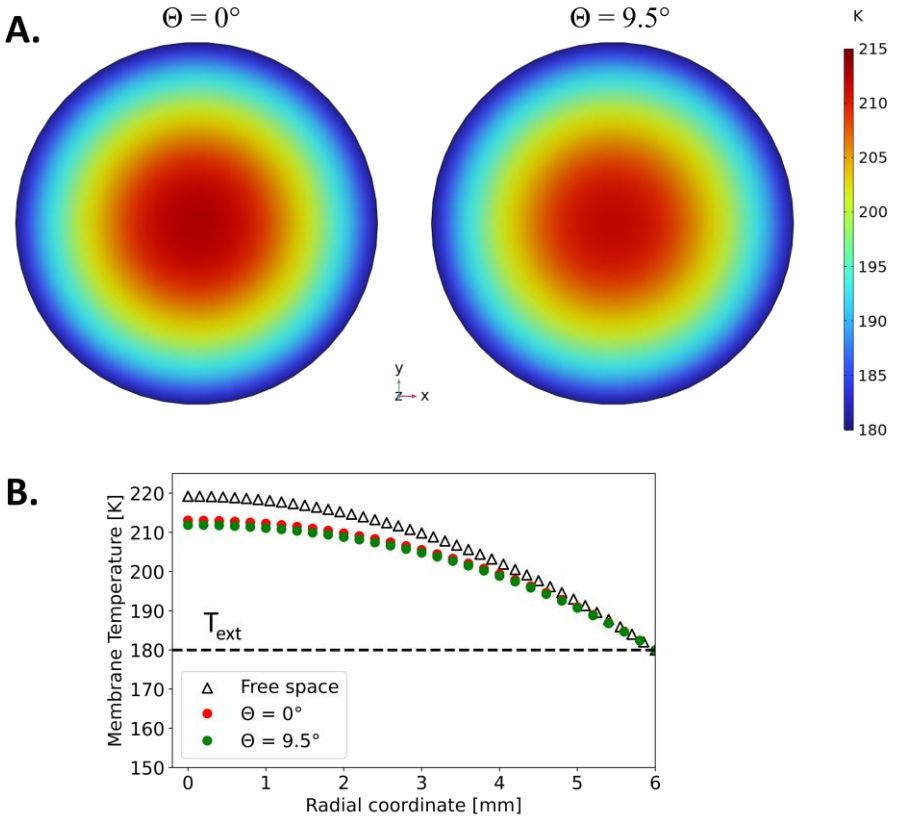

Fig S11: Finite elements simulation of the membrane's temperature as a function of the cavity alignment. A. 2D thermal profile of the membrane within the cryogenic cavity in the aligned configuration ($\theta = 0°$) and in the maximum misaligned configuration employed in the experiment ($\theta = 9.5°$). **B.** Membrane's thermal profile along the radial coordinate for the two alignment conditions. The cold finger temperature (T_{ext}) and the mirrors temperature have been set to 180 K.

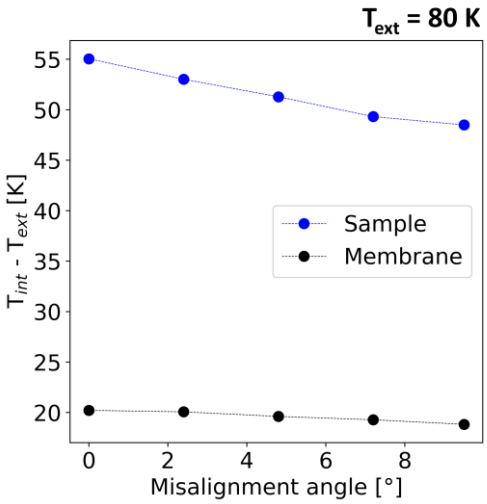

Fig S12: Temperature measurements within the cavity (11.5 GHz) as a function of the cavity alignment. In blue the dependence of the difference between the temperature measured on the sample (T_{int}) and on the cold finger (T_{ext}) as a function of the mirror alignment. In black, for comparison, the same differential temperature $T_{int} - T_{ext}$ measured on the membranes. For the presented measurements we set the cold finger at T_{ext} = 80 K.

d. Does the external radiation influence the sample temperature?

In order to prove that the shift of the effective critical temperature upon tuning the cavity resonance is not an effect merely due to the geometry of the cavity chamber, we removed the cavity mirrors and tracked the phase transition of the sample in free space at two different positions of the mirrors mounts (Fig. S13). For this characterization we compared the mirrors mounts distance corresponding to a 9 mm (16.7 GHz) cavity with the one corresponding to a 1 mm (150 GHz) cavity. No significant shift of the effective critical temperature (~ 2.0 K) is measured between the two configurations. This proves that the thermal load on the sample is not influenced by the distance from the cryogenic mirrors mounts, and hence that the effective critical temperature shift upon tuning the cavity mode (Fig. 4A of the main manuscript) cannot be trivially ascribed to a geometrical variation of the cavity chamber. Therefore, the critical temperatures measured in free space discussed in the main manuscript (Fig. 1) effectively set the absolute free space reference for all the cavity-dependent studies.

We also demonstrated that the leading effect is not related to a geometrical screening of the black-body ambient radiation, whose amount within the cavity can be geometrically modified by tuning the mirrors distance. To exclude this scenario, we screened with metallic foils the cavity chamber and, by means of the micrometric Cr-Al junction, tracked the differential temperature between the sample and the cold finger as a function of the cavity frequency. Importantly, as highlighted in Fig. S14, a similar temperature trend is detected in both the shielded and non-shielded configurations. This, together with the evidence of Fig. S13, further validates that the reported evidence cannot be simply explained in terms of a geometrical screening of the ambient blackbody radiation and more likely hints at a scenario mediated by cavity electrodynamics.

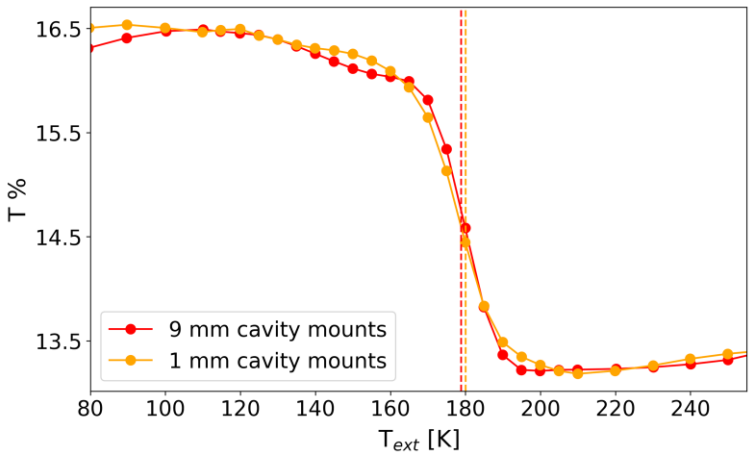

Fig S13: Dependence of the effective phase transition temperature on the cavity geometry (without mirrors). The low frequency transmission (0.2 THz < ω < 1.5 THz) in free space is plotted for two representative distances between the mirrors mounts and the sample. No significant shift in the effective critical temperature is observed (~ 2 K).

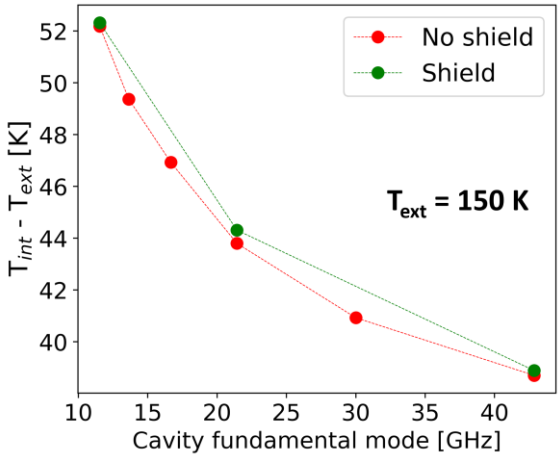

Fig S14: Effect of the shielding of ambient radiation on the sample's temperature. Differential temperature between the sample and the cold finger as a function of the cavity fundamental mode. Red (green) points correspond to sample temperatures measured without (with) shielding the cavity environment with alumina foils. The test has been made with the mirrors temperature set at 290 K.

e. Does the thermal load of the THz radiation affect the observed transition temperature?

In order to verify that the phase transition within the cavity is not influenced by the thermal load introduced by the THz radiation, we repeated the same temperature scan with different intensities of the THz pulse. This was achieved by varying the bias voltage of the photoconductive antenna. Fig S15 shows the cooling temperature scans for the sample within a cavity of a representative frequency of 36.8 GHz for two different peak strengths of the input THz field (0.1 KV/cm, and 0.03 KV/cm). A negligible shift of the effective critical temperature (< 1.0 K) is measured, confirming that the employed THz pulse only acts as probe and does not introduce a detectable thermal load at the sample position. For this reason, in order to maximize the signal to noise ratio of the detected THz field, all the measurements presented were performed at a THz input peak strength of 0.1 KV/cm.

A further confirmation of the negligible effect of the THz thermal load on the reported evidence is given by directly measuring the temperature of the membrane in the absence and in the presence of the THz field. In Fig. S16, we plot the temperature difference between the cold finger and the centre of the membrane (measured by means of the Cr-Al junction). We measured that even with the maximum THz intensity employed in all the measurements in the manuscript (0.1 kV/cm), the temperature difference $T_{Membrane} - T_{ext}$ changes by less than 1 K.

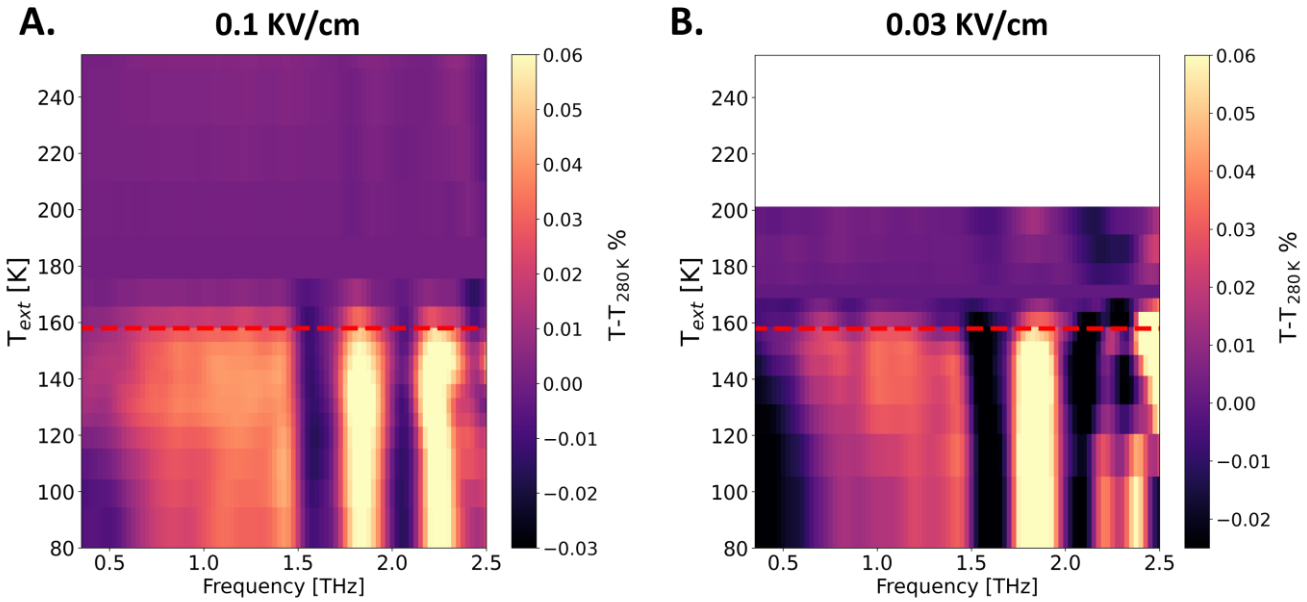

Fig S15: Dependence of the metal-to-insulator transition on THz probing intensity. Cooling temperature scans for the sample within a cavity of a representative frequency of 36.8 GHz for two different intensities of the THz probing field: 0.1 KV/cm (**A**) and 0.03 KV/cm (**B**). A negligible shift of the effective critical temperature (< 1.0 K) between the two THz intensities is detected.

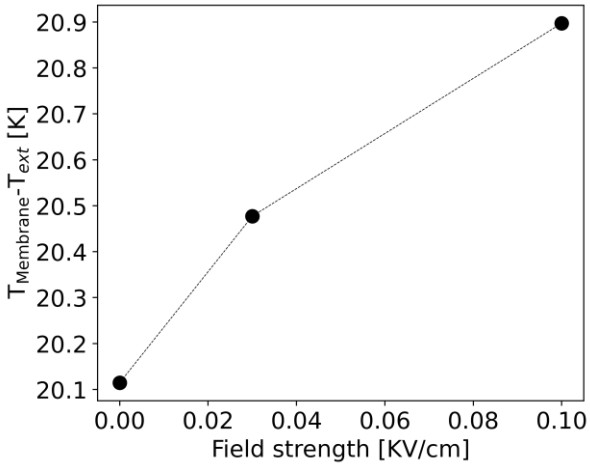

Fig S16: Dependence of the membrane temperature on the THz intensity. Measured difference between the temperature of the membrane and the temperature of the cold finger in the absence (0 kV/vm) and in the presence of THz radiation with two different intensities (0.03 and 0.1 kV/cm).

2. ADDITIONAL DATASETS

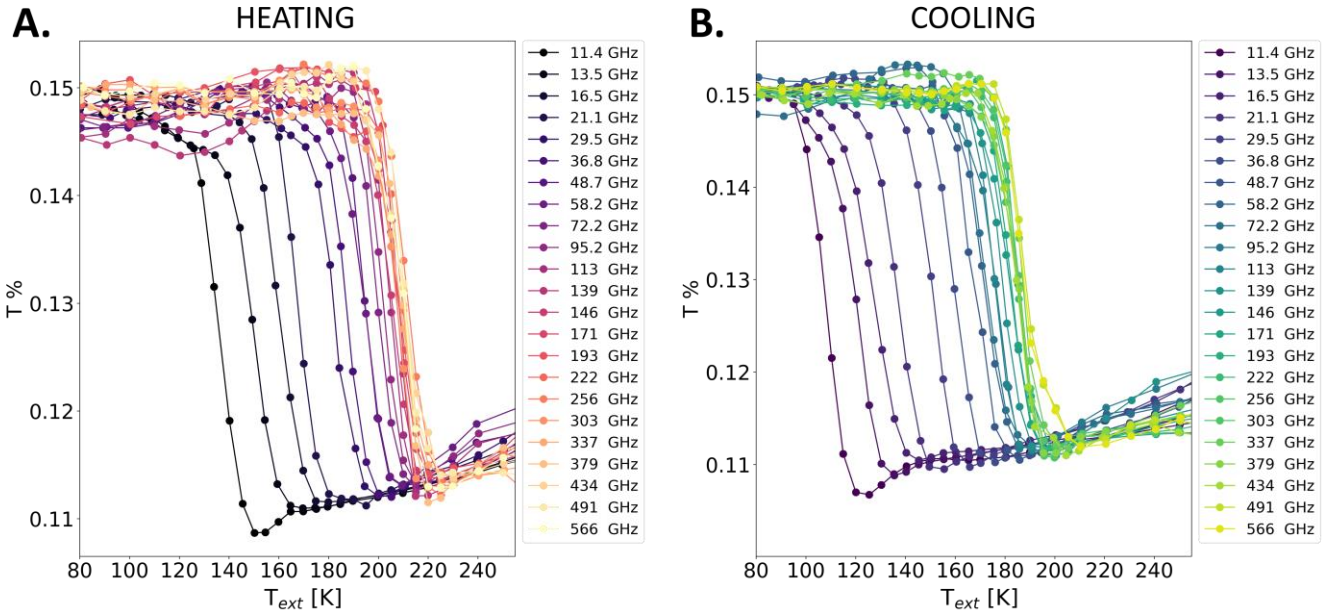

Fig S17: Raw temperature hysteretic curves as a function of the cavity frequency. A. Low frequency THz transmission ($0.2 < \omega < 1.5$ THz) for all the cavity frequencies of Fig. 4A (indicated in legend) measured upon heating the sample. B. Corresponding sweep curves for the cooling temperature scans.

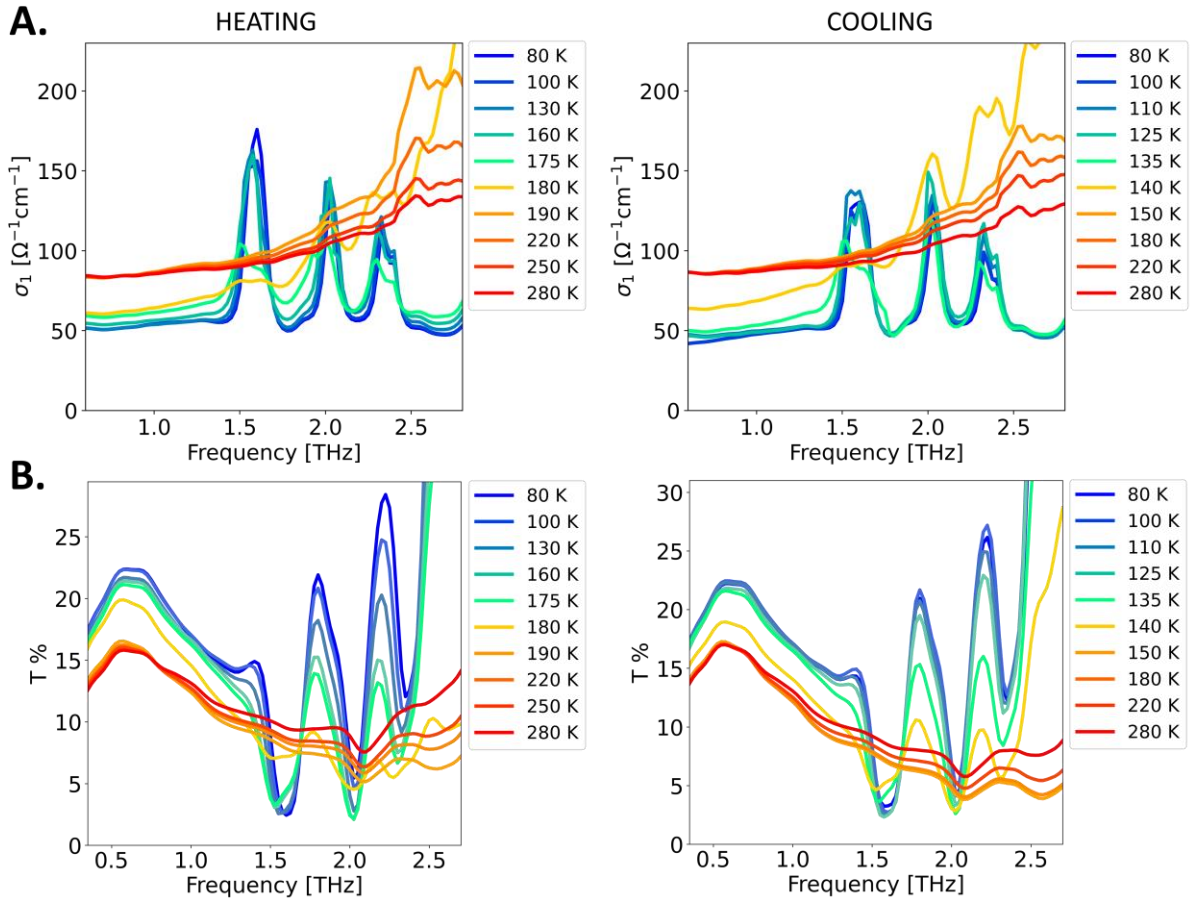

Fig S18: Optical conductivity and THz transmission in 1T-TaS_2 across the metal-to-insulator phase transition. A. Real part of the optical conductivity ($\sigma_1(\omega)$) measured in free space upon heating (left panel) and cooling (right panel) the sample from the insulating and metallic phase, respectively. B. THz transmission (T) measured in free space at different cold finger temperatures T_{ext} upon heating (left panel) and cooling (right panel) the sample.

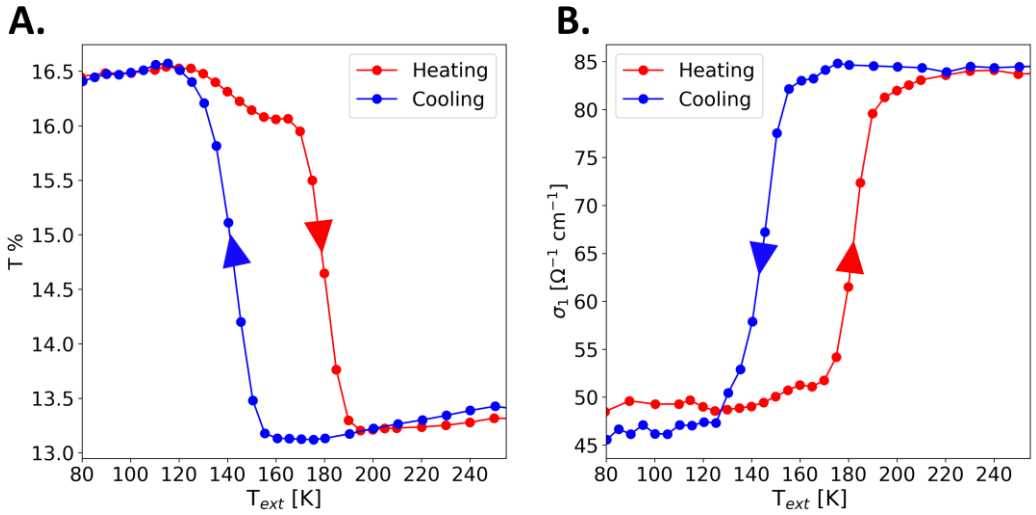

Fig S19: Hysteretic behaviour in THz transmission and optical conductivity. A. Low-frequency transmission ($0.2 < \omega < 1.5$ THz) upon heating and cooling the sample. B. Real part of the optical conductivity integrated in the same frequency range upon heating and cooling. The hysteretic behaviour is the same for both observables.

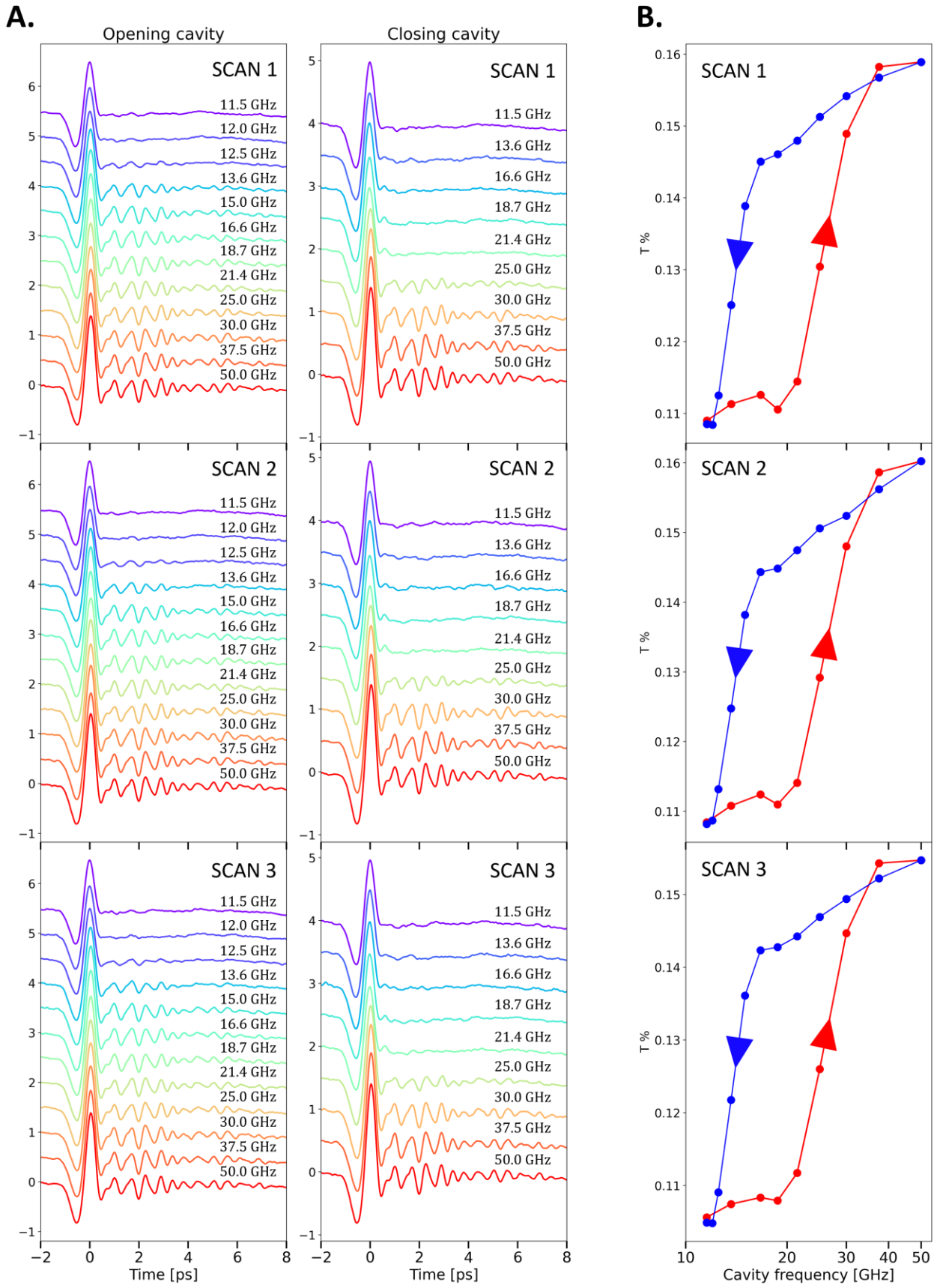

Fig S20: Single scans as function of the cavity length. A. Single THz fields measured upon opening (left) and closing (right) the cavity at a fixed temperature (150 K). The 3 consecutive scans employed for the average (insets of Fig. 3B) are presented. B. Corresponding low frequency transmission ($0.2 < \omega < 1.5$ THz) as a function of the cavity frequency for three consecutive scans. The hysteretic behaviour is reproducible for each single scan. The time from one scan and the next is approximately 10 minutes.

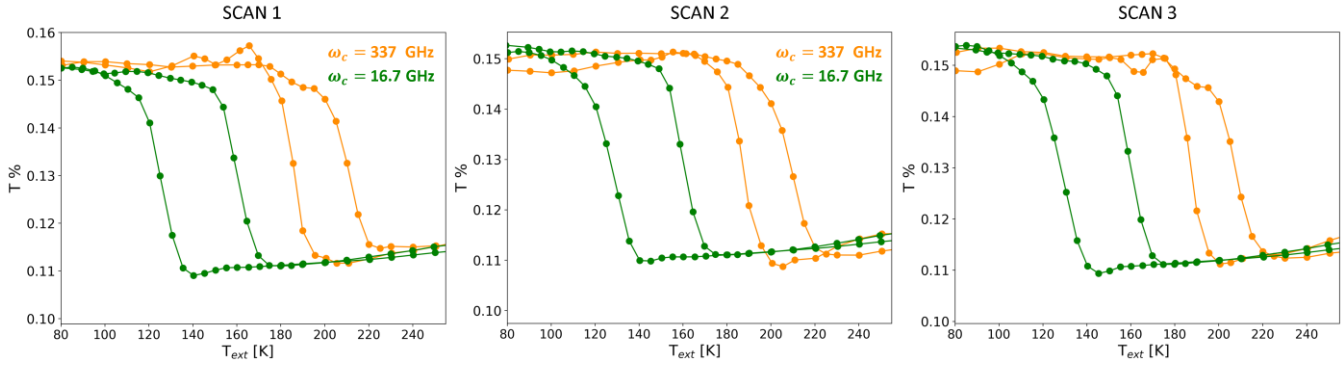

Fig S21: Single scans as function of temperature. Low frequency THz transmission as function of temperature (both heating and cooling) for two different cavity fundamental modes: 337 GHz (orange curves) and 16.7 GHz (green curves). The time from one scan and the next is approximately 10 minutes.

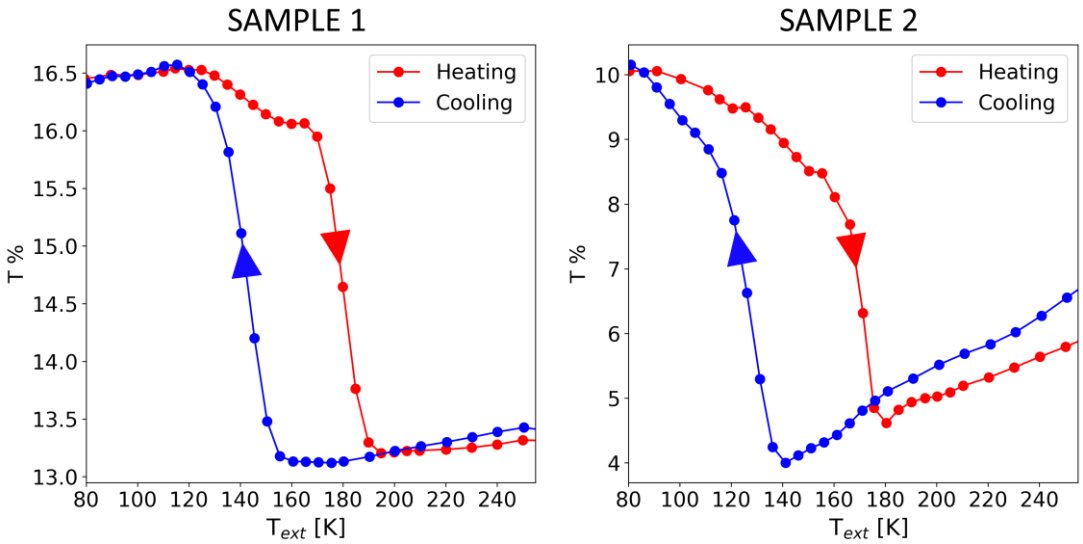

Fig S22: Hysteretic behaviour in different samples. Free-space hysteretic curves measured for two different samples belonging to the same batch. Sample 1 is the sample on which the measurements in the main manuscript have been performed.

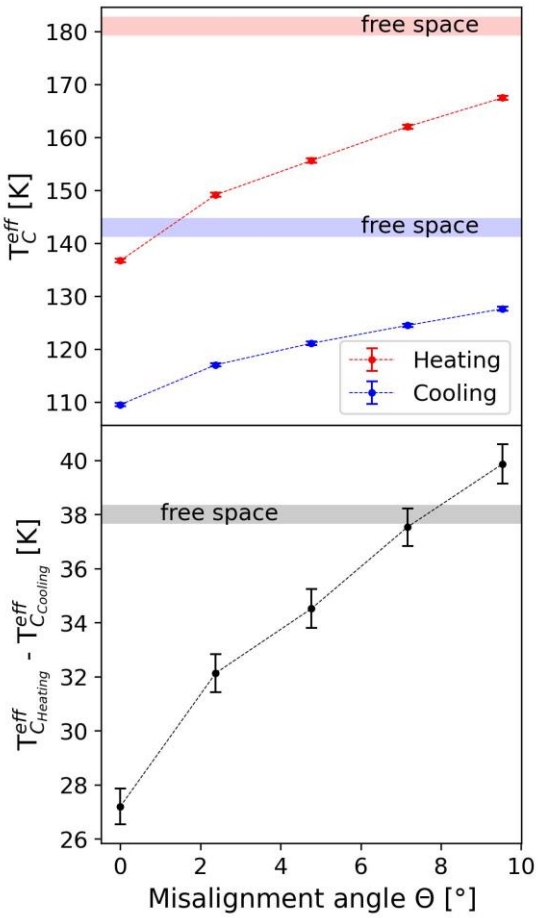

Fig S23: Effective critical temperature as function of the cavity alignment. Top panel: Effective critical temperature upon heating (red) and cooling (blue) the sample as function of the misalignment angle of the cavity. The shaded horizontal lines indicate the free-space reference. Bottom panel: corresponding hysteresis.